PHYSICAL REVIEW B **66**, 060505(R) (2002)

Shear fragmentation of unstable flux flow

Milind N. Kunchur,[1,*] Boris I. Ivlev,[1,2] and James M. Knight[1]
[1]*Department of Physics and Astronomy, University of South Carolina, Columbia, South Carolina 29208*
[2]*Instituto de Física, Universidad Autónoma de San Luis Potosí, San Luis Potosí, 78000 Mexico*
(Received 21 June 2002; published 15 August 2002)

When free flux flow is pushed beyond its instability, the homogeneous flow becomes spatially distorted leading to a new class of dynamic phases with steps in resistivity. At high-flux densities *B*, the relatively incompressible vortex matter fragments into domains of constant shear curvature, leading to a horizontal-sawtooth-shaped current-voltage characteristic. Measurements on $Y_1Ba_2Cu_3O_{7-\delta}$ films confirm this behavior and are quantitatively consistent with the model, which has no adjustable parameters.

DOI: 10.1103/PhysRevB.66.060505 PACS number(s): 74.60.Ge, 74.60.Ec, 74.60.Jg

In a type-II superconductor, a magnetic field H above the lower critical value H_{c1} introduces flux vortices containing an elementary quantum of flux $\Phi_o = hc/2e$. A transport current density j exerts a Lorentz driving force $\mathbf{F_L} = \mathbf{j} \times \mathbf{\Phi}_o / c$ on the vortices and the motion is opposed by a viscous drag $F_d = \eta v$, where η is the coefficient of viscosity and v is the vortex velocity. The system under study consists of a superconducting film in a perpendicular applied flux density B along $\hat{z}$, with j and the electric field $E = vB/c$ along $\hat{y}$ in the plane of the film. The transverse component of E is negligible for this discussion and v is predominantly along $\hat{x}$. (All equations are expressed in the Gaussian-cgs system and experimental quantities in practical units. Forces are defined per unit length per vortex except where noted otherwise. Material parameters refer to $Y_1Ba_2Cu_3O_{7-\delta}$ and are taken from standard references.[1])

Repulsive interactions between the vortices tend to align them into a uniform lattice and deviations from this lattice give rise to elastic forces. For our experimental geometry, the elastic forces per area on a plane of vortices by its neighboring planes are completely specified by the compressional and shear stresses:

$$X_x = c_{11}\left(\frac{\partial u}{\partial x}\right)$$

with

$$c_{11} = \frac{B^2}{2\pi(kd + \lambda^2 k^2)}, \tag{1}$$

$$X_y = c_{66}\left(\frac{\partial u}{\partial y}\right)$$

with

$$c_{66} = \frac{\Phi_0 B}{64\pi^2 \lambda^2}, \tag{2}$$

where c_{11} and c_{66} are the bulk and shear modulii, respectively,[2,3] λ is the magnetic penetration depth in the *ab* plane, d is the film thickness, and u is a displacement from equilibrium in the $\hat{x}$ direction; the stress and elastic-tensor coefficients have the standard meaning and the coordinate system moves with the local vortex velocity of the domain. In this work, pinning forces F_p are negligible (because $F_L \gg F_p$) and the steady-state motion reflects a balance between F_d, F_L, and F_e (the net elastic force): $j\Phi_0/c + F_e = \eta v$. At low dissipation levels $\eta \approx \Phi_0 H_{c2}/\rho_n = \text{const}$ and $F_e = 0$, resulting in free flux flow and an Ohmic response.

At high vortex velocities, η decreases leading to a negative differential conductivity and unstable motion. Figure 1 suggests a qualitative picture of how the drag force might vary with velocity. The initial positive slope ("A") at low v represents free flux flow. With increasing velocity, the electronic distribution function and/or electronic temperature becomes altered, causing η to diminish. The drag peaks at "B" and beyond this ("C") the slope is negative (the mechanism for the reduction of η with v is described elsewhere[4]). The drag rises again when v reaches some limiting value such as $v_\infty \sim \xi/\tau_\Delta$, where $\xi = 1.5$ nm is the coherence length and $\tau_\Delta = \hbar/\pi\Delta \approx 1.8 \times 10^{-14}$ s is the order-parameter relaxation time.

The drag function of Fig. 1 represents a *primitive* $j(E)$ curve, which the current density $j = c\eta v/\Phi_0$ (for $F_e = 0$) would follow for a hypothetical ensemble of uniformly arranged vortices with no elastic forces. The actual *macroscopic* $j(E)$ response will not follow this behavior: Upon encountering a negative slope, the vortex matter will become

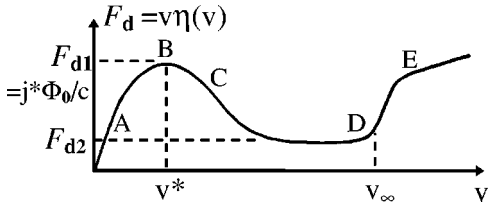

FIG. 1. Schematic diagram for the variation of the drag force $F_d = v\,\eta(v)$. The Lorentz driving force $F_L \equiv j\Phi_0/c$ equals F_d for a perfectly crystalline vortex distribution (up to "B"). At "B" the current density attains its peak value $j^* = cF_{d1}/\Phi_0$. Beyond "B," unstable dynamics destroy spatial uniformity and lead to a nonvanishing net elastic force $F_e = F_d - F_L$. Now vortices in differing elastic environments travel at unequal velocities on either positive slope "A–B" or "D–E." The upturn at "D" arises upon reaching some limiting velocity $v_\infty \lesssim \xi/\tau_\Delta$ and "E" is reached when the sample is driven normal.

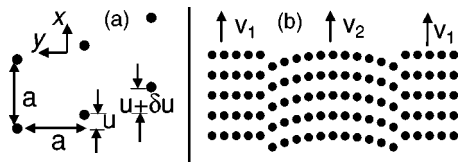

FIG. 2. (a) Vortex displacements of successive planes of vortices. A net elastic force results when there are unequal strains on the left and right sides (as shown), i.e., when $\partial^2 u/\partial y^2 \neq 0$. (b) Vortex positions calculated from Eq. (5) (with $\beta = 0.2$) showing a shear domain in which a higher velocity v_2, and consequent lower drag (F_{d2} in Fig. 1), is balanced by the extra elastic force. (A square lattice is shown for easier visualization but the equations in the text reflect the parameters for a triangular lattice.)

unstable and spatially distorted, so that vortices will travel at different velocities across regions of the sample with unequal elastic environments. This leads to a new class of dynamic phases in rapidly moving vortex matter. The range of stable vortex velocities lies on the positive slopes ''A–B'' and ''D–E'' in Fig. 1

In earlier work[5] we had explained descending-staircase $j(E)$ patterns in terms of compressional domains of reduced B. At low flux densities (~ 1 T) and intermediate temperatures ($\sim T_c/2$)—where such staircase patterns were most prominent—the Lorentz driving force $F_L/\text{area} = j\Phi_0/ca = 45\,000$ dy/cm^2 (with $j \sim 10^7$ A/cm^2 and $a = \sqrt{2\Phi_o/\sqrt{3}B} = 49$ nm for the vortex-lattice spacing) is stronger than the scale of compressional stress $X_x = 22\,000$ dy/cm^2 [from Eq. (1), taking $\lambda(0) = 140$ nm, $\lambda(T) = \lambda(0)(1-T/T_c)^{-1/2}$, $\partial u/\partial x \sim 1$, $k \sim 2\pi/a$, and $d = 90$ nm], permitting compressional modulations. The present work focuses on the high-B low-T regime where conditions are unfavorable for compressional strains (at 14 T, $F_L/\text{area} = 167\,000$ dy/cm^2 is weaker than $X_x = 636\,000$ dyn/cm^2). This leads to a completely different scenario from Ref. 5: Here the vortex matter fragments into transverse domains of unequal velocity stabilized by differential shear, as shown in Fig. 2 This idea will now be developed quantitatively.

Figure 2(a) shows a closeup view of shear strains in successive $\hat{x}$-$\hat{z}$ planes of vortices. For small strains, the net stress on the central plane from the vortices in the left and right planes is $X_{y,\text{net}} = c_{66}(a\sqrt{3}/2)(\partial^2 u/\partial y^2)$; the factor of $\sqrt{3}/2$ accounts for a triangular latice. Note that the stress-strain relationship of Eq. (2) is valid only for small strains $u \ll a$. The actual stress reaches a maximum when $u \approx a/4$ and vanishes at $u = a/2$ (when vortices of the central plane align between vortices of the left plane). For large shear strains, Eq. (2) can be generalized to $X_y = (c_{66}/\sqrt{3}\pi)\sin(\sqrt{3}\pi\partial u/\partial y)$, which has the required periodicity in u. This gives the net force per unit length $F_e = (a^2 c_{66}/2\pi)\partial[\sin(\sqrt{3}\pi\partial u/\partial y)]/\partial y$, and from which the force balance equation between F_e, F_d, and F_L is:

$$\left(\frac{\Phi_0^2}{64\sqrt{3}\pi^3\lambda^2}\right)\frac{\partial}{\partial y}\left[\sin\left(\sqrt{3}\pi\frac{\partial u}{\partial y}\right)\right] = v\,\eta - \frac{j\Phi_0}{c}. \qquad (3)$$

Any region of the system where $F_d \neq F_L$ will become elastically strained to make up the force difference. The sequence of events is as follows: Referring to Fig. 1, as the electric field across the system is increased from zero, the vortex matter remains uniform up to point ''B'' and all vortices move with the velocity $v = cE/B$. When v slightly exceeds v^*, a fluctuation will cause an entire plane of vortices to be accelerated to a velocity $v_2 \approx v_\infty$, where stability is regained upon encountering the positive slope at ''D.'' This faster moving plane will drag with it a finite-sized domain (of width W) as shown in Fig. 2(b), such that the relative shear displacements between adjacent planes satisfy Eq. (3). (The strong c_{66} at low T and high B facilitates a wide shear domain. At higher T, c_{66} weakens and the steps peter out, as is borne out by the data below.) There is a disproportionately large voltage drop $V_2 = v_\infty BW/c$ across the shear domain, reducing E in the bulk of the sample: The velocity v_1 in the bulk therefore drops below v^* to the region below ''B'' in Fig. 1. As the applied E is increased further, the vortex matter again reaches point ''B'' and a new shear domain is nucleated. The oscillatory excursions of the bulk vortex matter on the slope ''A–B'' (Fig. 1) lead to steps in the $j(E)$. Since B remains constant everywhere in this process, the macroscopic $j(E)$ curve will have a horizontal-sawtooth shape, with steps of width (noting that 1 km/s$\sim v^* \ll v_\infty \sim 100$ km/s)

$$\delta E = (v_\infty - v^*)WB/lc \approx v_\infty WB/lc, \qquad (4)$$

where l is the length of the sample.

We now calculate the shape and size of the shear domain, and hence the W that goes into the previous equations. A straightforward integration of Eq. (3) gives the function for the shear displacement u versus y, the position along the length of the sample:

$$u = -(\zeta \sin^{-1}\zeta + \sqrt{1-\zeta^2} - 1)/(\sqrt{3}\pi\beta), \qquad (5)$$

where $\zeta = \beta y$ and $\beta = 2\pi(j\Phi_0/c - v\,\eta)/(a^2 c_{66}) \approx 2\pi\Phi_0 j^*/(ca^2 c_{66})$ (see Fig. 1). Figure 2(b) shows the consequent arrangement of vortices plotted according to Eq. (5). The continuous negative shear curvature defined by Eq. (3) leads to a curved locus within $|\zeta| = |\beta y| \leqslant 1$. Outside $\zeta = \pm 1$, Eq. (5) has no solution and the domain terminates. Physically, as one moves away from the domain center [see Fig. 2(b)] the downward displacement of each subsequent vortex plane gets larger and larger to provide a net downward force on the preceding vortex plane to balance the deficit between F_L and F_d [right-hand side of Eq. (3)]. However, once the differential displacement δu between neighboring planes reaches a quarter of a lattice spacing, the force cannot increase any further and slippage occurs—demarcating the domain boundary. The lateral size of the shear domain is thus $W = 2|y_{\max}| = 2/\beta$:

$$W \approx \frac{ca^2 c_{66}}{\pi j^* \Phi_0} = \frac{c\Phi_0}{32\sqrt{3}\pi^3 j^* \lambda^2} \qquad (6)$$

and the horizontal width of the $j(E)$ steps is [combining Eqs. (4) and (6)]

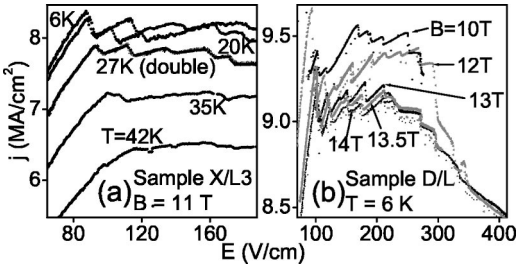

FIG. 3. Experimental $j(E)$ curves for two samples, showing horizontal-sawtooth-like shapes characteristic of shear fragmentation, favored at high values of B. The first peak arises from a vortex instability. Subsequent steps arise from the nucleation of shear domains. (a) Sample X/L3 at $B=11$ T and various T. With increasing T, the vortex instability softens and the steps wash out. (b) Sample D/L at $T=6$ K and various B. With increasing B and the c_{11}/c_{66} ratio, the steps evolve from a complicated pattern (mixed-mode fragmentation) to a more regular horizontal-sawtooth pattern (shear fragmentation). At $E \gtrsim 250$ V/cm, there is a switch in behavior to a descending-staircase shape, with all curves tending to converge together (characteristic of compressional distortions).

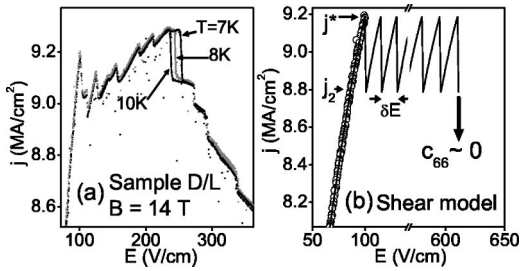

FIG. 4. (a) Experimental $j(E)$ curves for sample D/L at the lowest-T values and highest $B(=14$ T), where shear fragmentation is most favorable, showing conspicuous sawtoothlike patterns. The data also show clearly the sharp transition in behavior from a sawtooth to a descending-staircase pattern at around $E \sim 250$ V/cm, where the elastic moduli collapse due to a rise in the electronic temperature T'. (b) Theoretically calculated $j(E)$ characteristic based on the shear-domain model presented in the text. The model has no adjustable parameters. The vertical and horizontal sizes of the steps are of comparable magnitudes to the experimental values. The bold downward arrow indicates the calculated E where T' reaches T_c. Melting occurs at a value of E below this upper limit.

$$\delta E \approx \frac{v_\infty \Phi_0 B}{32\sqrt{3}\pi^3 l j^* \lambda^2} \sim \frac{\xi \Delta \Phi_0 B}{32\sqrt{3}\hbar \pi^2 l j^* \lambda^2}. \tag{7}$$

We now turn to the experimental details and results. The samples are c-axis-oriented epitaxial films of $Y_1Ba_2Cu_3O_{7-\delta}$ on (100) $LaAlO_3$ substrates with T_c's around 90 K and thickness $d \approx 90$ nm. Electron-beam lithography was used to pattern bridges of width $w \approx 5$ μm and length $l \approx 90$ μm. Three samples were studied carefully in the high-B and low-T regime to confirm the ubiquitous observation of the sawtooth-shaped step structures in the $j(E)$ curve in every case for $B \gtrsim 10$ T and $T \lesssim 30$ K. (Altogether the instability and various types of step structures were studied in 10 samples, at 12 temperatures: 1.6, 2.2, 6, 7, 8, 10, 20, 27, 35, 42, 50, and 80 K and at 13 flux densities: 0.1, 0.2, 0.5, 1, 1.5, 2, 10, 11, 13, 13.5, 13.8, 14, and 15.8 T. Due to lack of space a comprehensive presentation of the data systematics, along with a discussion of the full complement of effects occurring in high-velocity flux motion, will be deferred to a future review article.) The electrical transport measurements were made with a constant-voltage pulsed source, preamplifier circuitry, and a digital storage oscilloscope. The pulse rise times are about 100 ns with a duty cycle of about 1 ppm. Each $j(E)$ curve typically consists of 1000 separate data points and each point is an average of several hundred pulses, so that a single curve takes about a week to measure. The observed steps are perfectly reproducible and without hysteresis with respect to $j(E)$ being measured in increasing or decreasing E. This was checked extensively and Fig. 3(a) shows the 27-K data as one such ''double'' trace. The effective thermal resistances are of the order of a few nK cm^3/W. Note that the j values in the experiment are an order-of-magnitude lower than the depairing current density[6] and the applied flux densities exceed the self-field of the current by at least two orders of magnitude. Further details about the experimental techniques are discussed elsewhere.[7,8]

Figure 3 shows experimental $j(E)$ curves for two samples showing horizontal-sawtooth-like shapes characteristic of shear fragmentation. The first peaks in the data curves correspond to point ''B'' on the primitive curve (Fig. 1) and arise from a vortex instability.[4,9] Subsequent steps arise from the nucleation of shear domains. Figure 3(a) shows one sample (X/L3) at a fixed $B(=11$ T) and various T. With increasing T, the vortex instability softens and the steps wash out. Figure 3(b) shows another sample (D/L) at a fixed low T $(=6$ K) and various B. With increasing B and the c_{11}/c_{66} ratio, the steps evolve from a complicated pattern (mixed-mode fragmentation) to a more regular horizontal-sawtooth pattern (shear fragmentation). The data in Fig. 3(b) were measured with newer, more advanced electronics and thus extend to much higher electric fields. At $E \sim 250$ V/cm, there is a new feature corresponding to a sharp switch in behavior to a descending-staircase shape, with all curves converging together (characteristic of compressional distortions[5]). This transition may signify a melting of the vortex lattice and an abrupt drop in c_{66}.

Figure 4(a) shows a set of experimental $j(E)$ curves that examines more closely the low-T high-B regime ruled by shear fragmentation. The data show conspicuous sawtooth $j(E)$ patterns followed by the abrupt transition at $E \sim 250$ V/cm. The slightly upward trend of the sawtooth portion (exaggerated by the expanded y axis) and extra fine structure could be caused by speed-of-sound effects,[10] a slight shift in the instability break point with increasing E,[11] and higher-order elastic corrections.

We now compare these observations with the model. Inserting the typical $j^* \sim 9 \times 10^6$ MA/cm^2, $\xi = 1.5$ nm, $\Delta = 19$ meV, $B = 140\,000$ g, and $\lambda = 140$ nm into Eq. (7) gives $\delta E = 15$ V/cm. This is comparable to the experimentally observed step width of $\delta E \sim 25$ V/cm. From this calculated $\delta E = 15$ V/cm, one can construct the entire $j(E)$ behavior as shown in Fig. 4(b). The symbols show the primitive part ($j \leqslant j^*$, $E \leqslant E^*$) of the 8-K, 14-T experimen-

tal data [from Fig. 4(a)]. The solid line is the theoretical curve generated by retracing the segment between j_2 and j^* with successive offsets of δE along the E axis. As explained earlier, this portion of $j(E)$ is retraced each time a new shear domain is nucleated and the electric field in the bulk vortex matter is reduced by the amount δE. Note that the size of the steps along both axes is comparable to the experimental steps.

Finally we address the precipitous drop in $j(E)$ observed around $E \sim 250$ V/cm followed by the switch to a descending-staircase pattern: As the applied E is increased, the electronic temperature T' rises above the lattice phonon temperature T_p, which in turn rises above the bath temperature T_0 (a detailed discussion of these nonequilibrium shifts and the role of a nonthermal distribution function is given elsewhere.[4,9,11]) When T' rises to the vicinity of T_c, the vortex lattice melts and loses its shear modulus.[3] To obtain an order-of-magnitude estimate of this E, the nonequilibrium energy rise of the electronic system above the phonon temperature can be approximated by $\delta\epsilon \sim jE\tau_\epsilon$, where τ_ϵ is an average electron-phonon energy relaxation time. Since we start from $T \ll T_c$ and heat the electrons to close to T_c, $\delta\epsilon \sim H_c^2/8\pi$, where the right-hand side expression is the condensation energy and H_c is the thermodynamic critical field. Taking $H_c = 12\,000$ Oe, $j \sim 9\times10^6$ MA/cm^2, and $\tau_\epsilon \sim 10^{-10}$ s (Ref. 4), gives the upper bound $E \sim 600$ V/cm [shown by the large arrow in Fig. 4(b)], which is consistent with the observed value of $E \sim 250$ V/cm.

In conclusion we have investigated a new regime of strongly driven flux flow at high-flux densities, where the flux seems to fragment into shear domains beyond the low-temperature instability, causing sawtoothlike steps in the $j(E)$ curve. The experiment explores unprecedented values of power density ($>3\times10^9$ W/cm^3) and electric field (>400 V/cm), where a second transition is observed, beyond which the behavior switches to a descending-staircase pattern. Our estimated spatial scale of the elastic domains and consequent size of the $j(E)$ steps are consistent with the observations. We hope our study will encourage detailed theoretical work of these new dynamic phases that form in unstable flux flow. Besides their fundamental interest, the anticipation and full understanding of such regimes, where the resistivity rises catastrophically, is relevant to the thermal stability of practical conductors.

The authors acknowledge useful discussions and other assistance from M. Geller, D. K. Christen, J. M. Phillips, and A. Koshelev. This work was supported by the U. S. Department of Energy through Grant No. DE-FG02-99ER45763.

*Electronic address: kunchur@sc.edu; URL: http://www.physics.sc.edu/kunchur

[1] NIST WebHTS database http://www.ceramics.nist.gov/srd/hts/htsquery.htm; and C. Poole, H. A. Farach, and R. J. Creswick, *Superconductivity* (Academic Press, San Diego, 1995).

[2] E. Sardella, cond-mat/0002344 (unpublished).

[3] J. Blatter *et al.*, Rev. Mod. Phys. **66**, 1125 (1994), and references therein.

[4] M. N. Kunchur, Phys. Rev. Lett. (to be published).

[5] M.N. Kunchur, B.I. Ivlev, and J.M. Knight, Phys. Rev. Lett. **87**, 177001 (2001).

[6] M.N. Kunchur, D.K. Christen, C.E. Klabunde, and J.M. Phillips, Phys. Rev. Lett. **72**, 752 (1994).

[7] M.N. Kunchur, Mod. Phys. Lett. B **9**, 399 (1995).

[8] M.N. Kunchur, B.I. Ivlev, D.K. Christen, and J.M. Phillips, Phys. Rev. Lett. **84**, 5204 (2000).

[9] A.I. Larkin and Yu. N. Ovchinnikov, Zh. Éksp. Teor. Fiz. **68**, 1915 (1975) [Sov. Phys. JETP **41**, 960 (1976)].

[10] B.I. Ivlev, S. Mejia Rosales, and M.N. Kunchur, Phys. Rev. B **60**, 12 419 (1999); B.I. Ivlev, M.N. Kunchur, and S. Mejia Rosales, *ibid.* **64**, 024508 (2001).

[11] A.I. Bezuglyj and V.A. Shklovskij, Physica C **202**, 234 (1992).